Materials Science and Technology (MS&T) 2007
September 16-20, 2007, Detroit, Michigan · Copyright © 2007 MS&T'07®
MATERIALS AND SYSTEMS: International Symposium on Ceramic Matrix Composites
Organized by Narottam P. Bansal, Jitendra P. Singh, Sung R. Choi, and Aldo R. Boccaccini
Poster

In Situ Neutron Diffraction Study on the Effect of Aluminium Fluoride on Phase Transformation of Mullite from Alumina/Clay

N. Tezuka, I.-M. Low
Department of Imaging & Applied Physics, Curtin University of Technology, GPO Box U1987, Perth, WA 6845, Australia

I. Davies
Department of Mechanical Engineering, Curtin University of Technology, GPO Box U1987, Perth, WA 6845, Australia

I. Alecu, R. Stead
Rojan Advanced Ceramics Pty Ltd., PO Box 7126, Spearwood, WA 6163, Australia

M. Avdeev
The Bragg Institute, Australian Nuclear Science and Technology Organisation, PMB 1, Menai, NSW 2234, Australia

E. Mehrtens, B. Latella
Institute of Materials and Engineering Science, Australian Nuclear Science and Technology Organisation, PMB 1, Menai, NSW 2234, Australia

Keywords: Mullite, Additives, Kaolin, Neutron Diffraction, Young's Modulus

Abstract

The effect of aluminium fluoride (AlF_3) on the phase transformation sequence of mullite ($3Al_2O_3{\cdot}2SiO_2$) from two different types of kaolin (kaolinite and halloysite) ($Al_2Si_2O_5(OH)_4{\cdot}2H_2O$) within an alumina ($Al_2O_3$) matrix for a temperature range of 20 – 1500 °C was investigated using *in situ* neutron diffraction. Samples containing a mixture of AlF_3 (0 – 5 wt%), Al_2O_3 and kaolin were heated up to 1500 °C and then furnace cooled. During the heating procedure, one hour neutron diffraction scans were conducted at 600, 900, 1100, 1200, 1300 and 1400 °C, followed by six consecutive one hour scans at 1500 °C and finally a one hour scan at room temperature upon cooling. The diffraction patterns collected between 1100 and 1500 °C were analyzed by Rietveld analysis. The observed phase transformations exhibited a typical sequence found in clay/alumina ceramics. Corundum, mullite and cristobalite were observed. A common feature among the specimens containing different amounts of AlF_3 and kaolin was that the content of corundum decreased as the amount of mullite increased, whilst the cristobalite content tended to peak near the temperature where the amounts of corundum and mullite were approximately equal. The mullitization temperature was reduced as the AlF_3 content increased for both kaolinite and halloysite. The presence of AlF_3 appeared to reduce the onset temperature for mullite nucleation, which is at a much lower temperature compared to that of grain growth. However, AlF_3 also seemed to lower densification. Likewise mechanical properties of the resulting specimens were determined.

Introduction

Mullite is widely studied due to its excellent mechanical, thermal and chemical properties [1, 2]. Mullite is the only stable solid-solution within the $SiO_2 - Al_2O_3$ system and the chemical formula is generally described as $Al_2(Al_{2+2x}Si_{2-2x})O_{10-x}$ ($0.18 \leq x \leq 0.88$). The most common form of mullite is $3Al_2O_3 \cdot 2SiO_2$ ($x = 0.25$) which is sometimes known as "secondary mullite", however, $2Al_2O_3 \cdot SiO_2$ ($x = 0.40$) is also important and is often referred to as "primary mullite". When the fabricating conditions for mullite, *e.g.*, starting materials, precursors, sintering conditions, *etc.*, are carefully controlled, then the resulting mullite often exhibits a unique needle-like microstructure. A typical example of this is the use of clay materials and/or additives such as MgO and TiO_2 in order to enhance needle-like mullite formation by liquid phase aided thermal transformation [3-5]. This morphological feature has benefits not only for toughening by reinforcement of the matrix but also for the formation of whiskers; some workers have prepared elongated mullite through the use of seeding and template [6, 7].

However, despite the microstructural advantage, it is often difficult to obtain dense mullite or mullite composites without the use of sintering aids and resulting liquid phase sintering. Although oxides are the most common type of additive, workers have also noted that some alkali fluorides may reduce the sintering temperature of mullite [8]. Another effect of fluoride reported by others is the reaction caused by fluorine, namely, aluminium fluoride (AlF_3) was used to form a precursor for mullite whiskers, *i.e.*, AlOF, which later reacts with SiF_4 ($6AlOF + 2SiF_4 + 7/2O_2 \rightarrow 3Al_2O_3 \cdot 2SiO_2 + 14F$) [9]. AlF_3 was also reported to react in aluminosilicate to form topaz as an intermediate phase before mullite [10]. These mullitization mechanisms, *i.e.*, vapour-solid reaction and dissociation of topaz, are different from that found in liquid phase sintering. Some authors have reported that AlF_3 required a higher temperature for densification [11], probably due to an interlocking mullite structure.

The effect of AlF_3 on the mullitization process is not fully understood and the thermal transformation has rarely been investigated. Hence, the aim of this paper was to investigate the effect of AlF_3 on the thermal phase transformation behaviour using *in situ* neutron diffraction and to determine the mechanical properties as a function of mullite content of the alumina/clay ceramics.

Experimental Procedures

Kaolinite (Unimin Australia Ltd.) and halloysite (Imerys Tableware Asia Ltd., New Zealand) were utilized as the starting clay materials for this investigation with their respective chemical compositions being shown in Table 1. The major differences between these clays were: (i) kaolinite contained a higher proportion of impurities such as TiO_2 and Fe_2O_3 and (ii) halloysite contained a higher amount of cristobalite (SiO_2).

Six different starting materials were utilised for the *in situ* neutron diffraction experiments, each containing 44 wt% alumina and 56 wt% clay (kaolinite or halloysite) together

Table 1 Chemical composition of the clay minerals (wt%)

	SiO_2	Al_2O_3	Fe_2O_3	CaO	MgO	TiO_2	Na_2O	K_2O	LOI
Kaolinite	46.8	37.0	1.01	0.29	0.24	0.8	0.12	0.21	13.45
Halloysite	49.1	35.9	0.29	trace	trace	0.07	trace	trace	14.08

with different AlF_3 additive contents (*i.e.*, 0, 3 and 5 wt%). The powders were prepared by dry mixing. The green samples were prepared by uniaxial pressing at about 110 MPa followed by cold isostatic pressing at 200 MPa. Two cylindrical rod samples of diameter 15 mm and length 25 mm were utilised for each composition.

As the high water content of clay (typically 13-14 wt% for kaolin) often results in the formation of cracks during sintering, the samples containing AlF_3 additive for mechanical testing were prepared using metakaolin, which was dehydrated and dehydroxylated at 750 °C prior to mixing the raw materials. For these specimens the AlF_3 content was fixed at 3 wt% and compared with samples containing no AlF_3. Four different metakaolin levels (0, 5, 15 and 30 wt%) with the remainder of alumina were prepared by wet mixing in ethanol in order to examine the effect of AlF_3, clay content and sintering time.

The wet mixed powders were dried and shaped into rectangular bars of approximate size 12 x 60 x 8 mm and then uniaxially pressed at 110 MPa and then cold isostatically pressed (CIP) at 200 MPa prior to sintering at 1600 °C for 2 hrs using a heating rate of 1.5 $°C \cdot min^{-1}$ in air. In addition, the samples containing 30 wt% metakaolin and pure alumina were also sintered for 5 or 10 hrs. All of these samples were then hot isostatically pressed (HIPed) at 1600°C for 2 hr at 200 MPa. Table 2 shows the compositions and sintering conditions of the various samples.

In situ neutron diffraction of the specimens was conducted using the Medium Resolution Powder Diffractometer (MRPD) at the Australian Nuclear Science and Technology Organization (ANSTO) in Lucas Heights, New South Wales, Australia. A maximum temperature of 1500 °C available for the furnace was utilised. Each sample was scanned at 600, 900, 1100, 1200, 1300, 1400, and 1500 °C upon heating and at room temperature following air cooling. Each neutron diffraction spectrum was collected using a wavelength of 1.320 Å with a 2θ range from 5 to 135° in 0.1° steps in one hour scans except at 1500°C where six consecutive one hour scans were made. The Rietveld method [12] was used, in conjunction with the RIETICA software package [13], to quantify the phase abundance within sintered specimens. The mullite crystal structure model reported by Angel and Prewitt [14] was applied to the refinement. Refinements were started with the parameters from the following data: mullite (ICSD 66452), corundum (ICSD 73530), cristobalite (ICSD 74530) and γ-alumina (ICSD 95302).

Bulk density (D_b) and apparent porosity (P_a) were measured using the Archimedes method for each composition. The sintered bar samples were machined and the surface of each bar specimen was polished down to a 10 micron finish prior to mechanical testing; preliminary analysis showed that the strength-limiting flaw size was several times larger than this value. Five

Table 2 Summary of experimental conditions

Marks	Chemical Compositions (wt%)				Maximum Temperature (°C)	Holding Time (hr.)
	Alumina	Kaolinite	Halloysite	AlF_3		
AKF0, 3, 5	44	56	-	0, 3, 5	(1500)*	*
AHF0, 3, 5	44	-	56	0, 3, 5	(1500)*	*
Marks	Alumina	Meta-kaolinite	Meta-halloysite	AlF_3	Maximum Temperature (°C)	Holding Time (hr.)
AMK	100-70	0-30		0	1600	2, 5, 10**
AMKF	100-70	0-30		3	1600	2, 5, 10**
AMH	100-70		0-30	0	1600	2, 5, 10**
AMHF	100-70		0-30	3	1600	2, 5, 10**

* In-situ neutron scanning, ** additional 2 hrs by HIPing

bar samples were initially prepared for each composition but some of these delaminated after sintering or cracked during the machining process and could not be tested. The dynamic Young's modulus was determined using the impulse excitation method. For cases where the shear modulus could not be measured accurately due to porosity, *etc.*, the Poisson's ratio was assumed to be 0.22 (which is typical for alumina [15]). Four-point bend tests were generally performed using outer and inner spans of 40 and 20 mm, respectively, although for some cases values of 20 and 10 mm were used when the bar was not sufficiently long due to damage produced during sintering and/or machining. The four-point bend tests were conducted using a crosshead speed of 0.3 $mm \cdot min^{-1}$ on a servo-electric mechanical testing machine (Model 8562, Instron, Canton, MA).

Results and Discussion

In Situ Neutron Diffraction

Figure 1 shows the *in situ* neutron diffraction patterns obtained at 600 – 1500°C for alumina/kaolinite (Fig. 1 (a) – (c)) or alumina/halloysite (Fig. 1 (d) – (f)) with various levels of AlF_3 additive (0, 3 and 5 wt%). The observed phase transformations for all specimens followed a sequence typical for alumina/clay ceramics, *i.e.*, starting materials → metakaolin → Si – Al spinel or γ – alumina → mullite; mullite was the dominant final phase at 1500°C in this series of *in situ* study. Cristobalite once crystallized above the initial amount and almost completely dissolved later within the tested temperature range, *i.e.* up to 1500°C, as a common phenomenon in this phase transformation sequence. However, the temperature which gave the maximum peak intensity varied depending on the type of clay and the amount of AlF_3. The combination of alumina/kaolinite and 5 wt% AlF_3 exhibited the lowest temperature for mullite evolution at 900°C together with the maximum cristobalite peak (at 1100°C), whilst alumina/halloysite without AlF_3 showed the highest temperatures for mullite evolution (1200°C) and maximum cristobalite peak (1400°C). Topaz was not identified from the *in situ* diffraction patterns in this work and this was attributed to the amount of AlF_3 addition being too small.

The diffraction patterns for all samples scanned at 1100, 1200, 1300, 1400 and 1500 °C were analyzed using the Rietveld method and Rietica software. A summary of the resulting phase abundances has been shown in Fig. 2. The common feature among the different AlF_3 contents (0 – 5 wt%) and kaolin type (kaolinite or halloysite) is that the amount of corundum decreases as mullite increases, and that cristobalite tends to have its peak near the temperature where the lines for corundum and mullite cross.

As clearly shown in Fig. 2, the cross points between corundum and mullite are shifted towards lower temperatures as the AlF_3 content increases for both kaolinite and halloysite, however, halloysite is still inactive in terms of mullitization when compared to kaolinite. Temperatures corresponding to 50 % mullitization were estimated by interpolating the data in Fig. 2. Each temperature can be regarded as a relative mullitization onset temperature especially for grain growth after any nucleation stage. Fig. 3 shows the effect of AlF_3 on the 50 % mullitization temperature with AlF_3 being seen to be effective in lowering the mullitization temperature. It is also expected that AlF_3 decreases the onset temperature for mullite nucleation (which takes place at far lower temperatures when compared to grain growth).

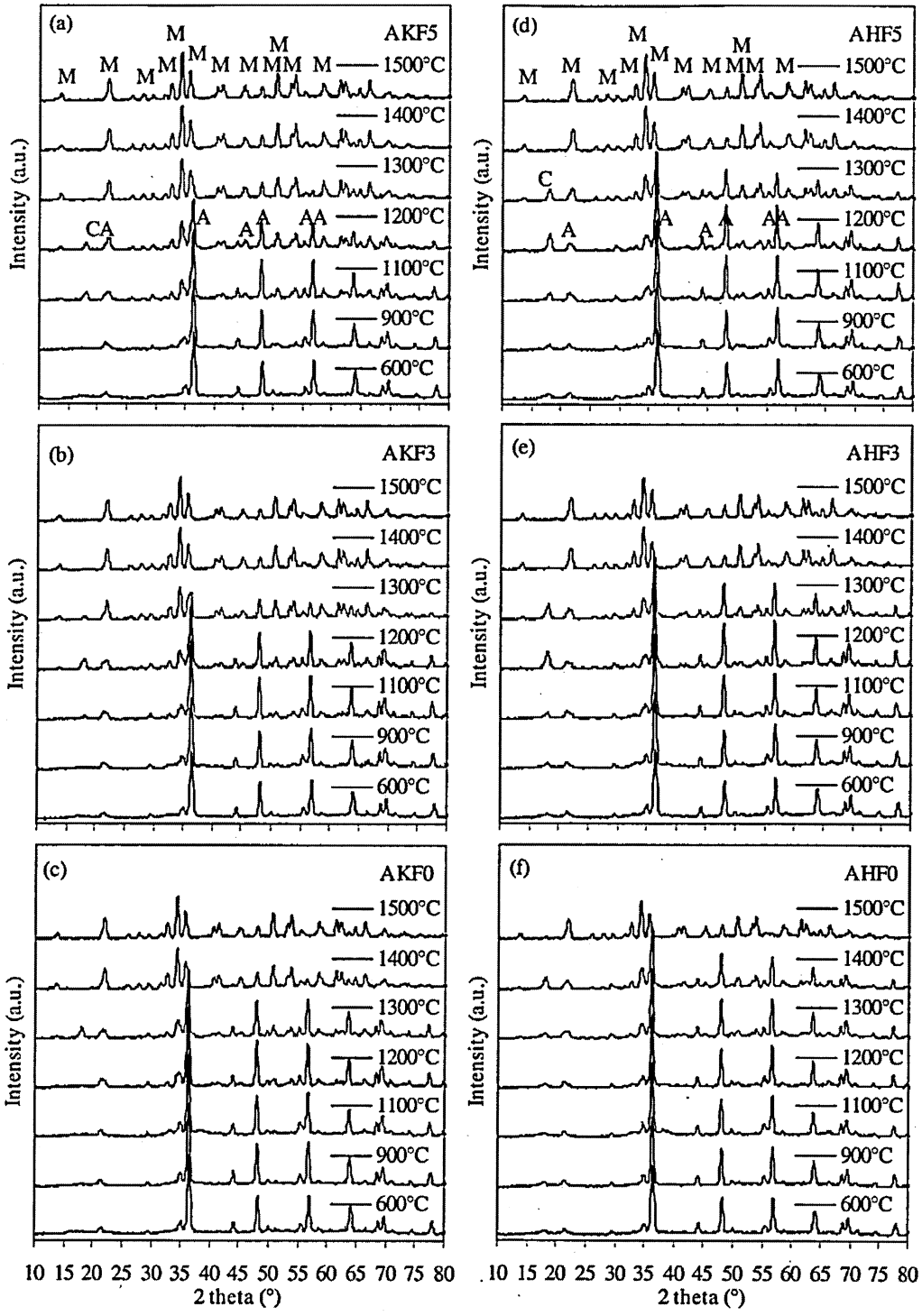

Figure 1 In situ neutron diffraction patterns of alumina/kaolinite (a - c) and alumina/halloysite (d - f) with various AlF_3 additive contents, 5wt% (a, d), 3wt% (b, e) and without AlF_3 (c, f) (M: mullite, A: corundum, C: cristobalite)

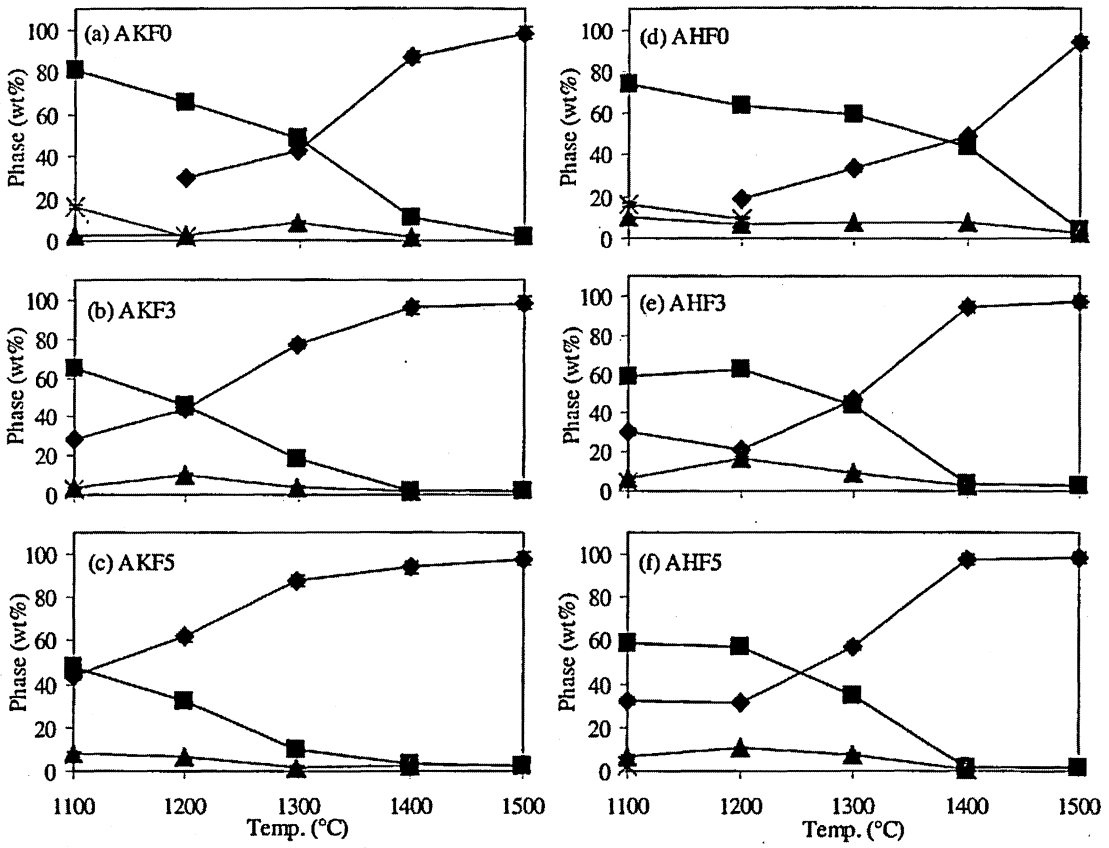

Figure 2 Effect of AlF_3 on in situ phase transformation in alumina/kaolinite (a - c) and alumina/halloysite (d - f) (AlF_3: 0 wt% (a, d), 3 wt% (b, e) and 5 wt% (c, f))

(♦ : Mullite, ■ : Corundum, ▲ : Cristobalite, X: γ-alumina)

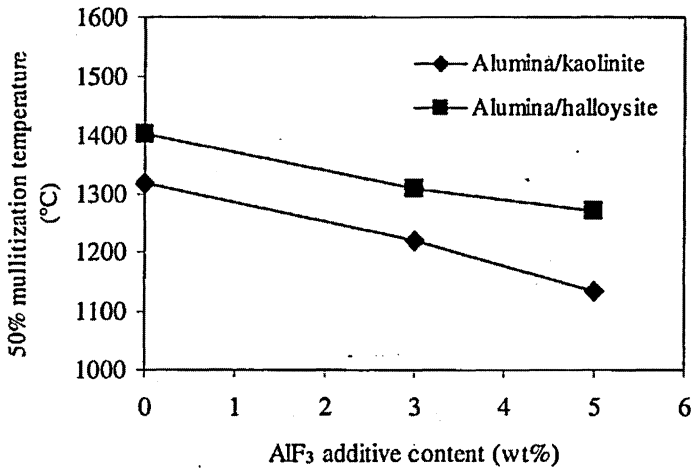

Figure 3 Effect of AlF_3 on mullitization temperature

Mechanical Properties

Figure 4 shows the influence of estimated mullite content and holding time at 1600°C on bulk density, apparent porosity, Young's modulus and flexural strength. Bulk density decreased as the estimated mullite content increased as shown in Fig.4(a). The difference of the measured bulk densities from the calculated true density increased with the estimated mullite content, and this effect was larger in the alumina/metahalloysite system; the low bulk density of this system was attributed to the high apparent porosity as shown in Fig. 4(b). This trend implied a low sinterability of mullite compared to alumina. AlF_3 was shown to increase porosity, however, the influence of the different clays (kaolinite and halloysite) on the bulk density and apparent porosity was larger than that of AlF_3 under the conditions of this work. Since AlF_3 does not induce a liquid phase, the different impurity contents in kaolinite and halloysite appear to have influenced the consequent densification; *i.e.*, higher impurity content of kaolinite resulted in higher bulk density. Young's modulus followed a similar trend as the bulk density (Fig. 4(c)), as might be expected, whilst flexural strength did not change significantly for specimens containing more than 30% of mullite (Fig. 4(d)). Hence, Young's modulus varies linearly in proportion to the ratio of alumina and mullite. On the other hand, the flexural strength remains relatively constant irrespective of the mullite content.

As shown in Fig. 4(e), the minimum holding time (2 hrs) at the maximum temperature (1600 °C) was not long enough to achieve full densification for all of the compositions. However, the relative densification to the theoretical density (alumina: 3.98 $g{\cdot}cm^{-3}$, mullite: 3.12 $g{\cdot}cm^{-3}$) was already 98% for pure alumina, and it decreased for alumina/clay compositions with or without AlF_3 as follows: 90% (AMK), 89% (AMKF), 77% (AMH) and 73% (AMHF). These relative densities were improved by further sintering for 10 hours at 1600 °C to 98% (AMK), 98% (AMKF), 86% (AMH) and 80% (AMHF). The low density of alumina/metahalloysite was due to the large amount of apparent porosity which has not reached saturation within 10 hrs. at 1600°C (Fig. 4(f)). Young's modulus after different holding times (Fig. 4(g)) appeared to be influenced by the bulk density as already seen in Fig. 4(c). Whilst flexural strength was constant despite the densification as shown in Fig. 4(h), it seems as if the weak mullite matrix was the strength limiting factor, although it is also possible that the mullite/alumina ratio increased as mullitization proceeded.

Young's modulus (E) can be expressed as a function of porosity by an empirical equation as follows [16]:

$$E = E_0 \exp(-bP) \quad (1)$$

where P is the volume fraction porosity, E_0 is Young's modulus when P=0 and b is constant. P is described by bulk density (D_b) and true density (D_t) as follows,

$$P = (1 - D_b/D_t) \quad (2)$$

Therefore, if Dt is constant under the same composition, Eqn (1) can be rewritten as follows:

$$lnE = BD_b + C \quad (3)$$

where $B = b/D_t$ and C is constant.

The relationship between D_b and E for different compositions and holding time are shown in Fig. 5(a) and (b), respectively. The relationship in Fig. 5(a) is not completely linear possibly due to the change of D_t depending on the ratio of mullite and alumina, whilst Fig. 5(b)

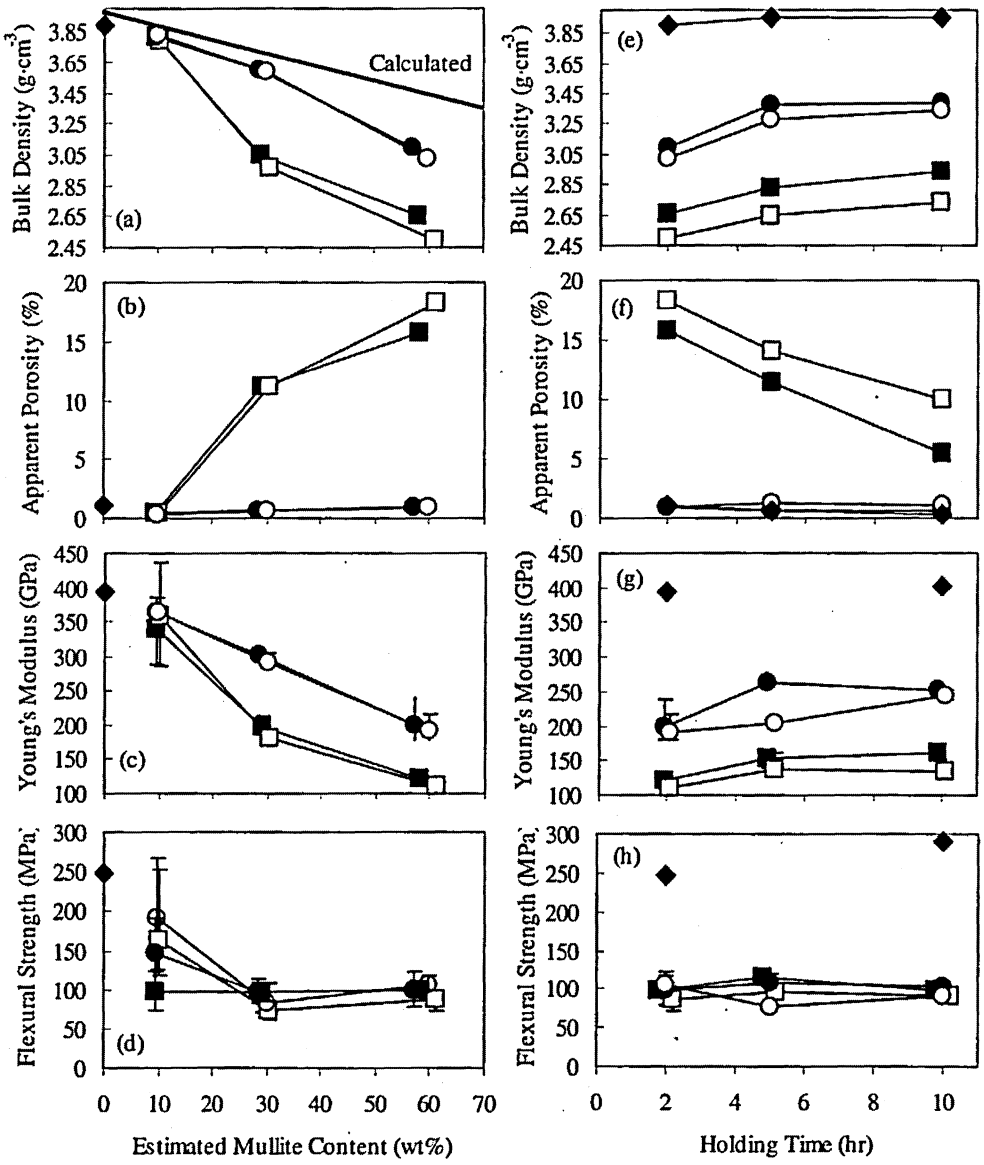

Figure 4 Effect of estimated mullite content (a - d) and holding time at 1600°C (e - h) on physical and mechanical properties

(a), (e): bulk density, (b), (f): apparent porosity, (c), (g): Young's modulus, (d), (h): flexural strength. Holding time of (a - d) is 2 hrs at 1600°C

(■: AMH, □: AMHF, ●: AMK, ○: AMKF, ♦: Alumina)

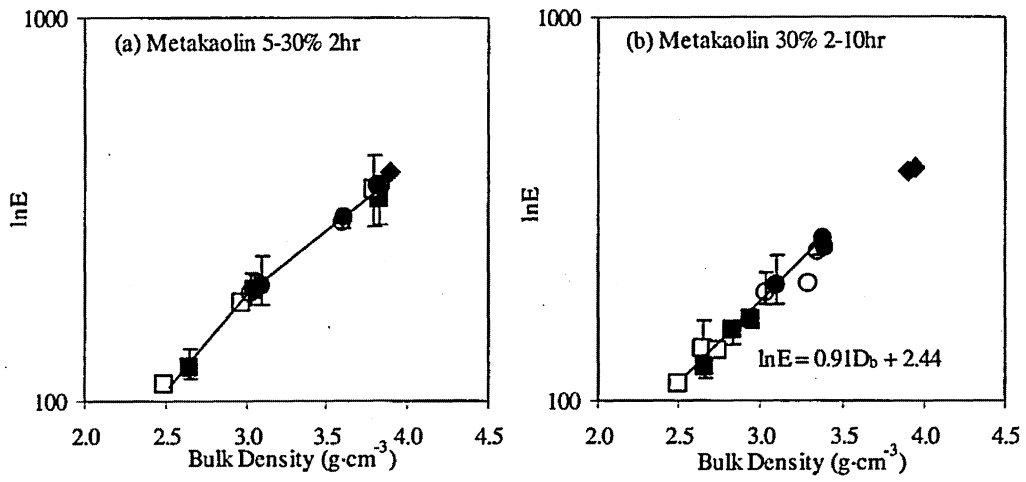

Figure 5 Relationship between bulk density and Young's modulus in different (a) compositions and (b) holding time

(■ : AMH, □ : AMHF, ● : AMK, ○ : AMKF, ♦ : Alumina)

shows a linear correlation of the data with Eqn (3). When D_t is assumed to be approximately 3.4 g·cm^{-3} as estimated from the compositions, *i.e.*, 70 wt% alumina and 30 wt% metakaolin with or without AlF_3, the slope of Eqn. (1), *i.e.*, *b*, is 3.1 (± 0.2) which is close to the result of 3.03 found by previous researchers for mullite [17].

Conclusions

The effect of aluminium fluoride (AlF_3) on the thermal phase transformation and sinterability of alumina/clay ceramics was investigated and can be summarised as follows:

1. The transformation sequence for specimens containing AlF_3 followed the typical model for mullitization from kaolin. The main phases observed at the low (<1200°C), medium (1200-1300°C) and high temperature ranges (>1300°C) were (1) corundum, γ-alumina (or Si-Al spinel) and cristobalite, (2) mullite, corumdum and cristobalite, (3) mullite and corundum, respectively. AlF_3 reduced the mullitization temperature in both alumina/kaolinite and alumina/halloysite.

2. AlF_3 tends to suppress densification in alumina/metakaolin ceramics, but the degree of deterioration in terms of density is much larger between kaolinite and halloysite. Young's modulus had a good correlation with the bulk density for various alumina/mullite ratios and densification. However, flexural strength was considered to be controlled by the weakest area regardless the density when the estimated mullite content is more than 30 wt%.

Acknowledgments

This work was supported by the Australian Institute of Nuclear Science and Engineering (AINSE Awards 06110 and 06112).

References

[1] S. Somiya and Y. Hirata, Mullite Powder Technology and Applications in Japan, *Am. Ceram. Soc. Bull.*, Vol. 70 (No. 10), 1991, p 1624-1632.

[2] H. Schneider et al., Structure and Properties of Mullite – A Review, *J. Eur. Ceram. Soc.*, 2007, In Press, doi:10.1016/j.jeurceramsoc.2007.03.017

[3] C. Chen, G. Lan and W. Tuan, Microstructural Evolution of Mullite during the Sintering of Kaolin Powder Compacts, *Ceram. Int.*, Vol. 26, 2000, p 715-720.

[4] L. Kong et al., Effect of Alkaline-Earth oxides on Phase Formation and Morphology Development of Mullite Ceramics, *Ceram. Int.*, Vol. 30, 2004, p 1319-1323.

[5] S. Hong and G. Messing, Anisotropic Grain Growth in Diphasic-Gel-Derived Titania-Doped Mullite, *J. Am. Ceram. Soc.*, Vol. 81 (No. 5), 1998, p 1269-1277.

[6] S. Hong and G. Messing, Development of Textured Mullite by Templated Grain Growth, *J. Am. Ceram. Soc.*, Vol. 82 (No. 4), 1999, p 867-872.

[7] I. Gönenli and G. Messing, Texturing of Mullite by Templated Grain Growth Alminium Borate Whiskers, *J. Eur. Ceram. Soc.*, Vol. 21, 2001, p 2495-2501.

[8] N. Tezuka et al., Effect of Fluoride and Oxide Additives on the Phase Transformations in Alumina/Clay Ceramics, *J. Aust. Ceram. Soc.*, In Press.

[9] J. Meng et al., Microstructure and Mechanical Properties of Mullite Ceramics Containing Rodlike Particles, *J. Eur. Ceram. Soc.*, Vol. 18, 1998, p 1107-1114.

[10] A. Abdel-Rehim, Thermal Analysis of Topaz Synthesis from Kaolinite, *Thermochimica Acta*, Vol. 340/341, 1999, p 377-386.

[11] K. Okada and N. Otsuka, Synthesis of Mullite Whiskers and Their Application in Composites, *J. Am. Ceram. Soc.*, Vol. 74 (No. 10), 1991, p 2414-2418.

[12] H. Rietveld, A Profile Refinement Method for Nuclear and Magnetic Structures", *J. Appl. Cryst.*, Vol. 2, 1969, p 65-71.

[13] B. Hunter and C. Howard, A Computer Program for Rietveld Analysis of X-ray and Neutron Powder Diffraction Patterns, Lucas Heights Research Laboratories, Australian Nuclear Science and Technology Organization, February 2000

[14] R. Angel and C. Prewitt, Crystal Structure of Mullite: A Re-examination of the Average Structure, *Am. Mineral.*, Vol. 71, 1986, p 1476-1482.

[15] W. Callister, Jr., *Materials Science and Engineering An Introduction*, John Wiley & Sons, 2003, p 744.

[16] R. Spriggs, Expression for Effect of Porosity on Elastic Modulus of Polycrystalline Refractory Materials, Particularly Aluminum Oxide, *J. Am. Ceram. Soc.*, Vol. 44 (No. 12), 1961, p 628-629.

[17] R. Penty, D. Hasselman and R. Spriggs, Young's Modulus of High-Density Polycrystalline Mullite, *J. Am. Ceram. Soc.*, Vol. 55 (No. 3), 1972, p 169-170.